J Mater Sci (2008) 43:207–211
DOI 10.1007/s10853-007-2139-z

Evolution of microstructure, texture and grain boundary character in a severely cold rolled Ti + Nb IF steel

Rajib Saha · R. K. Ray

Received: 19 February 2007 / Accepted: 4 September 2007 / Published online: 28 September 2007

Abstract Severe cold rolling (up to 99.5% reduction) of a Ti + Nb IF steel has been found to produce nano-sized to ultrafine grains. The γ fibre intensity increases with the level of cold deformation. The fraction of high angle grain boundaries increases with increasing rolling reduction and then levels off at the highest deformation level. The coincidence site lattice boundary fraction increases continuously with increase in the amount of cold rolling.

Introduction

It has been reported that severe plastic deformation by methods such as Equal Channel Angular Pressing (ECAP) [1–5] and Accumulative Roll Bonding (ARB) [6, 7] is capable of producing nano-sized to ultrafine grained metallic materials. Other methods by which grain refinement can be achieved are ball milling (BM) [8, 9], high-speed drilling [10] and folding and rolling [11]. Specific thermo-mechanical processing techniques have also reported the production of fine grain size [12, 13]. Although the microstructure, texture and grain boundary character of steels processed by above techniques are known to some extent, the development of these parameters after applications of very high strains by the conventional cold rolling process in interstitial free (IF) steel has been rarely reported [13–15]. The present work describes the microstructural and textural evolution in a severely cold rolled Ti + Nb IF steel.

R. Saha (✉) · R. K. Ray
Department of Materials and Metallurgical Engineering, Indian Institute of Technology, Kanpur 208016, India
e-mail: rajib.saha@tatasteel.com; rajib31@gmail.com

R. Saha · R. K. Ray
R&D Division Tata Steel Limited, Jamshedpur 831001, India

Experimental

The steel, melted as an industrial heat, has the chemical composition: 0.003% C, 0.36% Mn, 0.006% S, 0.014% P, 0.012% Si, 0.047% Al, 0.0033% N, 0.011% Nb and 0.05% Ti (in wt%). A transfer bar of this steel was 80% controlled hot rolled in several passes to a final thickness of about 6 mm. The hot bands were then subjected to cold rolling by 90% ($\varepsilon = 2.3$), 98% ($\varepsilon = 3.92$) and 99.5% ($\varepsilon = 5.3$). A block of the size 150 × 75 × 6 mm was cut out from the hot rolled transfer bar and this was cold rolled 90% in an instrumented 4-high cold rolling mill having 150 mm diameter work rolls and 350 mm diameter back-up rolls. The rolling speed was 60 m/min and the lubricant used was a synthetic oil. The rolled sheet was cooled by a water jet. Coupons of sizes 60 × 20 × 0.6 mm were cut out from the 90% cold rolled steel and these were subjected to further cold rolling (to 98% and 99.5% total reduction) in a laboratory with 2-high rolling mills having a roll diameter of 127 mm, running at 72 rpm. The rolled sheets were cooled immediately in water at room temperature. Machine oil was used as a lubricant during rolling. Transmission electron microscopy (TEM) of thin foils was carried out using a JEOL 200-kV TEM and crystallographic textures were determined from the mid thickness regions of the cold rolled sheets using a FEI-Quanta 200 SEM, coupled with an EBSD facility using TSL software. During data collection, a minimum of seven Kikuchi bands were recorded to index a pattern, thus ensuring very reliable information. It has been reported by Field [16] that EBSD patterns having confidence index

above 0.1 can correctly index an orientation 95% of the time. In the present work, the average confidence index of the patterns was above 0.45 and this led to more than 97% of the patterns to be indexed correctly in every case. The average image quality of the patterns was more than 65, which also ensured that the patterns were properly indexed. The minimum angular resolution of the EBSD from alpha iron using W-filament has been reported to be 1° [17]. In order to make accurate measurements, misorientations less than 1.5° were excluded from the data in the present case. Orientation distribution functions (ODFs) were computed using the TSL-OIM software, and $\Phi_2 = 45°$ sections (Bunge notation) were determined therefrom. Using the same software the grain boundary character distributions as well as misorientation distribution maps were also determined. Dislocation density was calculated from Vickers microhardness values according to the procedure used by Yin et al. [18].

Results

Figure 1a–c show the misorientation maps of the steel, subjected to 90, 98 and 99.5% cold rolling. It is clear that with increasing amount of cold deformation, from 90 to 98% fraction of high misorientation boundaries (>15°) increases drastically and then stabilizes and remains nearly unchanged after further cold rolling (up to 99.5%).

TEM of large number of thin foils from the 98% and 99.5% cold rolled materials reveal the existence of very small nanometer range strain-free grains at many places. Initially it was thought that these were mainly recovered cells or sub-grains, separated from one another by low-angle grain boundaries. However, by tilting of the foils in the TEM it was realized that most of these are indeed very small strain-free grains. Figure 2a represents one such area from a very thin foil of the 98% ($\varepsilon = 3.92$) cold rolled material (rolling plane section). The selected area diffraction pattern (SADP) for the grains within the circled region is shown as an inset. It is clear that this SADP shows spot patterns from a number of grains. The sizes of most of the grains have been found to vary from 50 to 150 nm. Figure 2b represents the TEM microstructure of the 99.5% cold rolled material (rolling plane section). Here again a large number of nanosize grains have been observed. The SADP of the encircled area shows diffraction patterns for a large number of grains. The average grain size here varies between ~40 and 120nm. At a few places, signs of the beginning of coalescence of grains have also been observed.

The $\Phi_2 = 45°$ sections of the ODFs of the 90, 98 and 99.5% cold rolled IF steel are shown in Fig. 3a–c. All these plots show typical BCC rolling texture consisting of both RD (α) and ND (γ) fibres along with some amount of the rotated cube component. The intensity of α fibre has been generally found to strengthen continuously with increasing amount of cold rolling. Similarly the γ fibre also becomes more intense with increasing amount of rolling deformation. The γ and α fibre plots are presented in Fig. 4a, b. Cold rolling by an amount of 99.5% sharpens the γ fibre

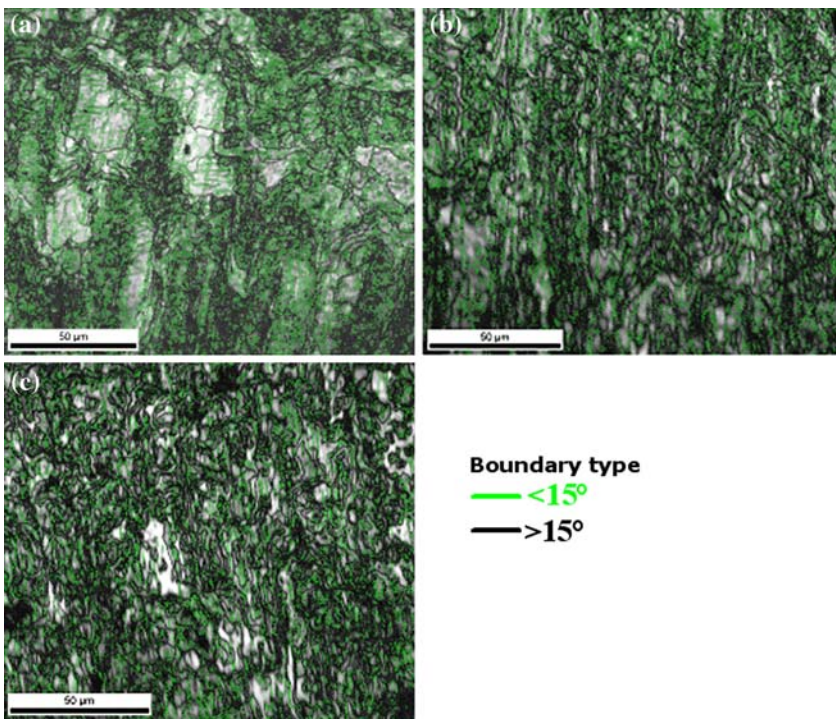

Fig. 1 Grain boundary misorientation maps of the 90%, 98% and 99.5% cold rolled IF steel respectively

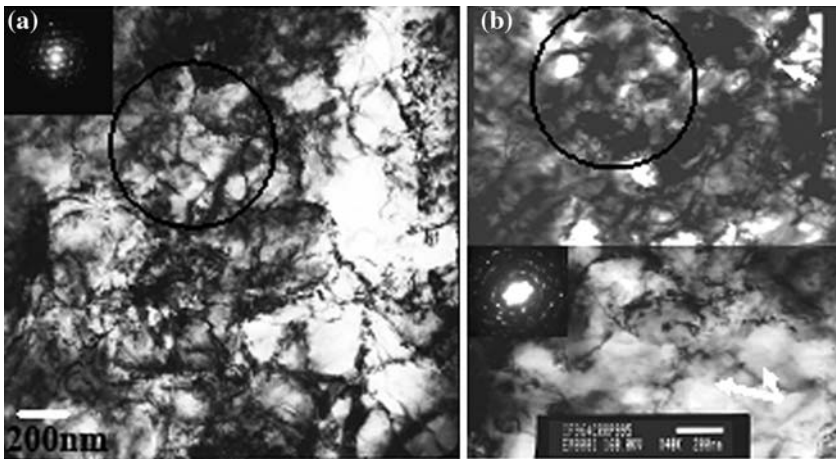

Fig. 2 TEM micrograph of the cold rolled IF steel (**a**) 98%, (**b**) 99.5% respectively

appreciably, specially at the orientation {111}<110>. The highly intense α fibre formed after 98% cold rolling becomes perceptibly weaker after 99.5% cold rolling.

The grain boundary character distribution (GBCD) plots for the steel sheets subjected to different cold rolling reductions are shown in Fig. 5a–c. There is a drastic decrease in the fraction low-angle boundaries (LAGB) and a corresponding sharp increase in the coincidence site lattice (CSL) and high-angle grain boundaries (HAGB) as the amount of cold rolling increases from 90 to 98%. The fractions of the different types of boundaries do not change much after 99.5% cold deformation. In fact, there is a slight increase of CSL fraction and a little decrease in the high-angle boundary fraction when rolling reduction increases from 98 to 99.5%.

Discussion

It would be tempting to correlate the formation of microstructure and texture and the evolution of grain boundaries as a function of the amount of cold rolling reduction. In general, an increase in the LAGB fraction has been associated with the formation of a strong texture [19–21] and of cells or sub-structures [22]. Accumulation of dislocations [23, 24] and formation of new grains, as in the case of recrystallization [25, 26], have been considered responsible for any increment in the HAGB fraction. An increase in the CSL fraction has been attributed to the refinement of the structure due to severe deformation [27].

The results of the present investigation have clearly shown that increasing the amount of cold rolling leads to the formation of a sharper texture. This is accompanied by an increase of the HAGB and CSL fractions and a decrease of the LAGB fraction. The continuous accumulation of dislocations across the boundaries due to heavy rolling reductions appears to be primarily responsible for this behaviour, and this seems to overshadow the effect of the increase of the texture sharpness which causes an increment of LAGB fraction. There can be another reason for the increase in HAGB fraction with increase in cold rolling reduction. TEM studies on a large number of thin foils of the cold rolled samples clearly indicated the formation of a large number of strain-free nano-sized to sub-micron grains after 98% and 99.5% cold deformation.

Yin et al. [18] suggested that the cell size continuously decreases due to continuing deformation, and dislocation density of the cell walls increases, thereby causing an increase in the average cell wall energy. After reaching a certain cell size, the cell structure will no longer be stable due to its higher energy. If this energy exceeds that of a typical grain boundary, then the accumulation of

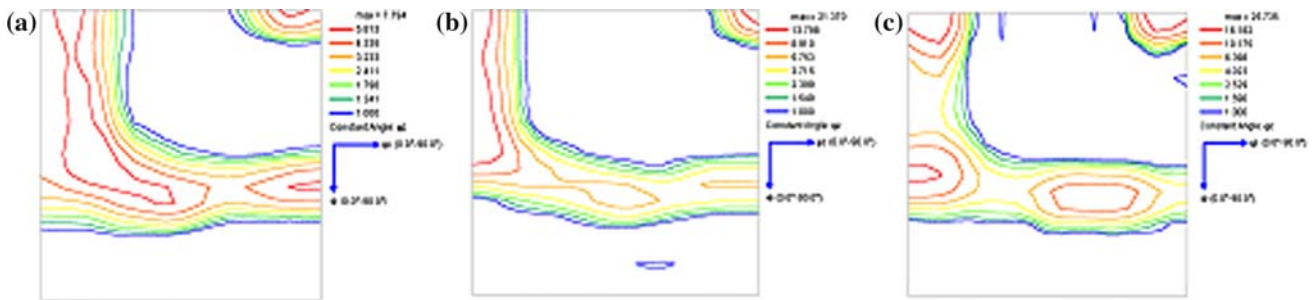

Fig. 3 $\Phi_2 = 45°$ sections of the ODFs of different amounts of cold rolled IF steel (**a**) 90%, (**b**) 98% and (**c**) 99.5%

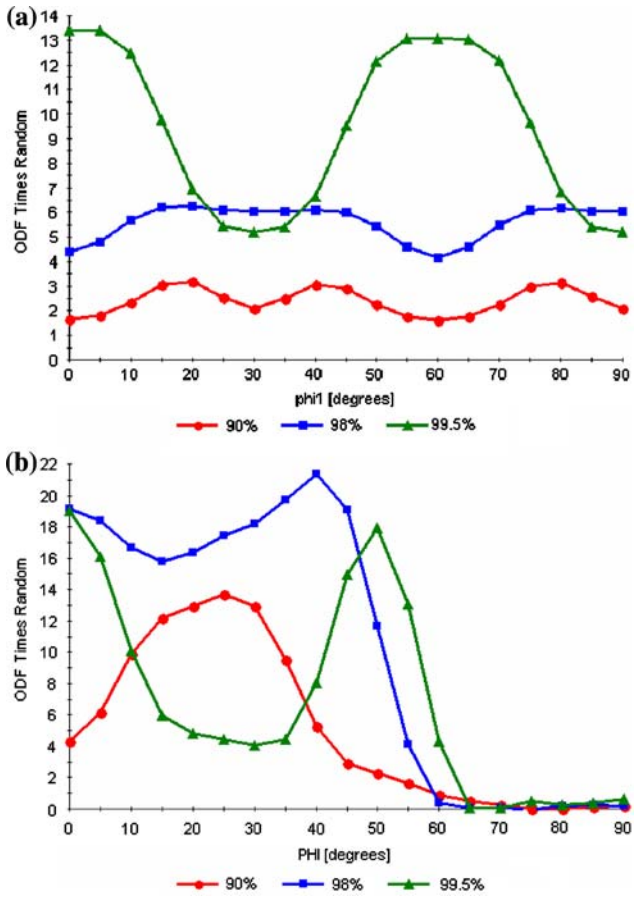

Fig. 4 Texture fibre plots of different amounts of cold rolled steel (**a**) γ fibre and (**b**) α fibre

dislocations in the cell wall will lead to the formation of a grain boundary instead. Yin et al. suggested that for this process to happen the total dislocation density of the material has to exceed a critical value of 2.5×10^{15} m^{-2}. The calculated dislocation density for the 99.5% cold rolled steel in the present investigation is 2.2×10^{15} m^{-2}, which is quite close to the above critical value. Thus it can be expected that heavy cold rolling reductions may lead to the formation of very small grains with high-angle boundaries. This will contribute to an increase in the HAGB fraction with increase in the amount of cold rolling. The apparent decrease in the HAGB fraction after 99.5% cold rolling from its value after 98% cold rolling can be attributed to growth of the sub-micron or nano-sized grains which has frequently been observed. Using an in situ dark-filed TEM technique, frequent rotation of nanocrystals (d $\sim$6 nm) into larger aggregates of neighbouring grains during deformation has been reported [8]. It is suggested that this may be due to the mechanism for the growth of submicron or nano-sized grains that have been observed in the present investigation.

Conclusion

Cold rolling of a Ti + Nb IF steel by heavy amounts (up to 99.5% reduction) appears to produce a large number of nano-sized to ultrafine grains. The general level of texture intensity and the sharpness of the γ fibre increases with increasing cold rolling reduction. The fraction of high

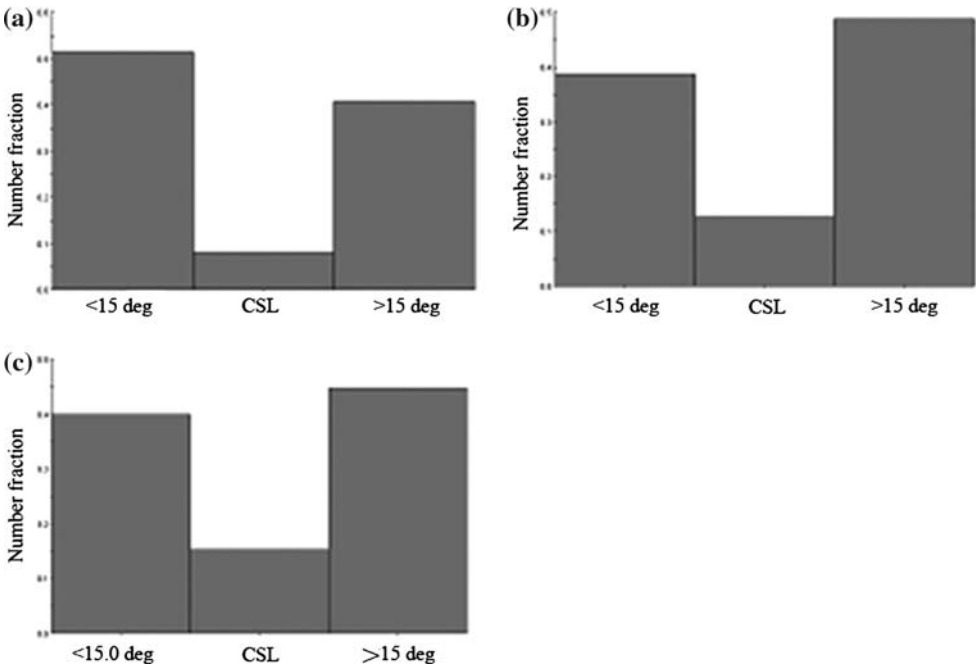

Fig. 5 Grain boundary character distribution plots of (**a**) 90%, (**b**) 98% and (**c**) 99.5% cold rolled steel

misorientation boundaries increases as the amount of cold rolling increases from 90 to 98%, and the levels off after 99.5% cold reduction. The CSL boundary fraction increases continuously with an increase in the amount of cold reduction. Growth of a few nano-sized and ultrafine grains has been observed after 99.5% cold rolling.

References

1. Valiev RZ, Korznikov AV, Mulyukov RR (1992) Phys Met Metallogr 73:373
2. Segal VM (1995) Mater Sci Eng A197:157
3. Valiev RZ, Islamgaliev RK, Alexandrov IV (2000) Prog Mat Sci 45:103
4. Iwahashi Y, Horita Z, Nemoto N, Longdon TG (1998) Acta Mater 46:3317
5. Farase S, Segal VM, Hartwig KT, Goforth RE (1997) Metals Mater Trans A 28A:1407
6. Saito Y, Utsunomiya H, Tsuji N, Sakai T (1999) Acta Mater 47(2):579
7. Saito Y, Tsuji N, Utsunomiya H, Sakai T, Hong RG (1998) Scripta Mater 39:1221
8. Shan Z, Stach EA, Wiezorek JMK, Knapp JA, Follstaedt DM, Mao SX (2004) Science 305:654
9. Liu ZG, Fetch HJ, Xu Y, Yin J, Tsuchiya K, Umemoto M (2003) Mat Sci Eng A362:322
10. Li JG, Umemoto M, Tadoka T, Tsuchiya T (2006) Mat Sci Eng 435–436:383
11. Dinda GP, Rosner H, Wilde G (2005) Mat Sci Eng 410–411:328
12. Belyakov A, Kimura Y, Tsuzaki K (2005) Mat Sci Eng A403:249
13. Reis ACC, Kestens K, Houbaert Y (2001) Proc. 22nd Risk Symposium on Material Science. Dinesen AR, Eldrup M, Juul Jensen D, Linderoth S, Pedersen Riso TB (eds). National Labortaory, Roslkilde, Denmark, p 383
14. Zaho X, Jing TF, Gao YW, Qiao GY, Zhou JF, Wang W (2005) Mat Sci Eng A397:117
15. Li BL, Godfrey A, Meng QC, Liu Q, Hansen N (2004) Acta Mater 52:1069
16. Field DP (1997) Ultramicroscopy 1–9:67
17. Humphreys FJ (2004) Scripta Materialia 51:771
18. Yin J, Umemoto M, Liu ZG, Tsuchiya K (2001) ISJ Int 41:1389
19. Randle V (1996) The role of the coincidence site lattice in grain boundary engineering. The Institute of Materials, ISBN 1-86152-006-1
20. Watanabe T (1992) Scripta Metallurgica 27:1497
21. Watanabe T, Arai KI, Terashima H, Oikawa H (1994) Solid State Phenom 34–38:317
22. Ivanisenko Y, Valiev RZ, Fetch HJ (2005) Mat Sci Eng A390:159
23. Hughes DA, Hansen N (1997) Acta Mater 45(9):3871
24. Hughes DA, Hansen N (1995) Scripta Metallurgical et aterialia 33(2):315
25. Humphreys FJ, Prangnell PB, Bowen JR, Gholinia A, Harris C (1999) Phil Trans R Soc 357:1663
26. Humphreys FJ, Hatherley M (2002) Recrystallization and related annealing phenomena, 2nd edn
27. Watanabe T (1992) Scripta Metallurgica 27:1497